

## Research Article

# Augmented photovoltaic performance of Cu/Ce-(Sn:Cd)/n-Si Schottky barrier diode utilizing dual-doped Ce-(Sn:Cd) thin films



T. Akila<sup>a</sup>, P. Gayathri<sup>a</sup>, G. Alan Sibu<sup>a</sup>, V. Balasubramani<sup>a,\*</sup>, Hamad Al-Lohedan<sup>b</sup>, Dhaifallah M. Al-Dhayan<sup>b</sup>

<sup>a</sup> Department of Physics, Saveetha School of Engineering, Saveetha Institute of Medical and Technical Sciences, Saveetha University, Chennai, 602 105, Tamil Nadu, India

<sup>b</sup> Department of Chemistry, College of Science, King Saud University, P.O.Box. 2455, Riyadh, 11451, Saudi Arabia

## ARTICLE INFO

**Keywords:**

Thin films  
MIS type Schottky barrier diode  
I-V characteristics  
Photodiode  
Optoelectronic applications

## ABSTRACT

In the current investigation, we are fabricated the Schottky barrier diode (SBDs) formed on dual doped Ce-(Sn:Cd) (1, 3 and 5 wt%) thin films. The film was prepared by spray pyrolysis of transparent glass and silicon substrates using a low-cost nebulizer, ideal substrate temperature is 450 °C and the structure, optics, morphology & electrical properties of the films were characterized by X-Ray Diffractometer, Atomic Force Microscope and Ultra Violet - Visible spectral, electrical and I-V properties of diodes. All dual doped thin films are the cubic structure, as revealed by the XRD pattern. Then the roughness and smoothness of the film were then revealed by atomic force microscopy (AFM). Ultraviolet-vis spectroscopy is formed on optical absorption and band gap energy (3.91 eV) also electrical conductivity increases Cd concentration of films corresponding activation energy diminish. Current-voltage properties [I-V] and photodiode parameters of Cu/Ce-(Sn:Cd)/n-Si diodes were evaluated in the dark and light. The barrier height ( $\Phi_B$ ) for the diode fabricated was initiate to be 0.69 eV, as well as ideality factors (n) 2.57 of the diode parameters. As a consequence, the 5 wt% of Cd parade greater device performance for the photodiode applications, the present study is first combination of dual doped samples and low cost JNSP technique.

## 1. Introduction

SBDs is a semiconductor device that plays an important role in electronic circuits and has special features and advantages over traditional diodes. Named after German physicist Walter H. Schottky, who contributed to the understanding of semiconductor physics, SBDs were characterized by their fast switching and low forward voltage also simplest form of the SBDs consists of MS junction, unlike the p-n junction in conventional diodes. A metal (usually a refractory metal such as platinum, tungsten or molybdenum) forms a barrier with a semiconductor material (usually silicon or gallium arsenide). This MS junction forms a Schottky barrier, which gives the diode its unique properties and working principle of the Schottky barrier diode. Its reasonable features based on fast optical response, ultra-high speed, low leakage current, stability and long lifetime led the research community to focus their research on the photon-focused device [1]. Electrons with more energy than the metal diffuse into the semiconductor, causing a depletion region this makes it possible to block the efficiency of the

diode material and provides faster conduction than conventional diodes. SBDs solar cells, sensors, photodetectors, frequency multipliers etc. Due to their use, they have become competitors in the field of micro/nano electronics technology [2–5]. An important advantage of Schottky barrier diodes is their low forward voltage, usually in the range of 0.2–0.4 V reduce power loss and increase the efficiency of various electrical applications. Absence of minority carriers at the MS junction allows fast switching, making SBDs suitable for high-frequency applications such as RF (radio frequency) circuits and electrically using devices. Many authors have reported that the SBDs can be achieved using metal and semiconductor layers [6–11]. SBDs have good temperature performance compared to conventional diodes and this feature makes them suitable for applications, where temperature is important. SBDs has a metal-semiconductor transition point whose properties depend on the material, band gap, morphology, dopant concentration coating between the metal and semiconductor [12]. SBDs are used in many areas including power rectification, signal demodulation, voltage compression and RF signal detection their ability to handle high frequencies and

\* Corresponding author.

E-mail address: [balasubramaniv3@gmail.com](mailto:balasubramaniv3@gmail.com) (V. Balasubramani).

fast transients makes them unique in today's electronics field. Smolyakov he studied the effect of interface of MIS devices [13]. MIS devices stand as pivotal components in modern electronics, offering a versatile and efficient platform for a limitless of applications. V. Rajagopal Reddy [14]. Structured diodes based on the MIS configuration play a critical role in electronic circuits, providing a bridge between metals, insulating materials and semiconductors. Tan MIS models with and without associated processes analysed [15]. MIS structures are the main components of semiconductor devices in this configuration allows the semiconductor to be replaced by applying voltage to the metal electrode, When electricity is used, it causes electric current in the circuit also affects the charge distribution in the semiconductor region underneath then the insulation layer is used to prevent the flow of electricity between metal and electrical equipment, except in special cases determined by the utility provider. MIS standards are widely used in integrated circuits, electronic devices other electronic devices to enable control of electrical properties such as conductivity and capacitance, which are important in the operation and operation of modern electronic devices. This comprehensive overview delves into the principles, applications and advantages of MIS device structured diodes, highlighting their significance in the ever-evolving landscape of electronic technologies. It seems that there is an inorganic interlayer at the MS interface that can replace the negative electric current of MIS type SBDs due to the significant tunnelling current [16]. Generally speaking, there are sturdy covalent bonds among atoms in the inorganic semiconductor lattice, it can increase a charging rate and therefore improve the performance of MIS diodes [17]. Due to the performance of MIS mainly depends on the nature of the interface process, the performance parameters and the height of the parameters, Changing the  $\Phi_B$  is particularly important has a significant impact on traffic flow, usually this is done by placing an insulating layer between metal contact and the semiconductor substrate [18]. Ali Baltakesmez [19].

Cerium (Ce), symbol Ce and atomic number 58, is a versatile chemical element exhibiting diverse properties. It rapidly oxidizes to form cerium oxide ( $\text{CeO}_2$ ) and displays multiple oxidation states, primarily  $\text{Ce}^{3+}$  and  $\text{Ce}^{4+}$ . Cerium salts are generally soluble, forming compounds ranging from oxides to coordination complexes. V. Balasubramani like as they also taken pure compound Ce [20]. Renowned for catalytic properties, especially as cerium oxide, it acts in industrial processes like catalytic converters. With fluorescent properties, radioactivity and the ability to form complexes, cerium finds applications in analytical chemistry. Y. Tian as they used as pure materials Ce [21]. By using the pure compound Ce, we can get good efficiency. Tin (Sn), atomic number 50, is a versatile metallic element. It forms tin oxide ( $\text{SnO}_2$ ), showcasing corrosion resistance. With oxidation states  $\text{Sn}^{2+}$  and  $\text{Sn}^{4+}$ , tin commonly exists in compounds like tin (IV) oxide, used in polishing powders and glass production. M. A. Pinheiro similarly, doped Ce with  $\text{SnO}_2$  [22]. Utilized in alloy formation, such as bronze, tin's chemical versatility includes halide compounds, acid reactivity and amphoteric behaviour. Malleable and ductile, tin finds use in catalysis and corrosion-resistant plating, impacting industries from electronics to food packaging. After adding the doped material Sn, it enhanced the electrical properties. Cadmium (Cd), with atomic number 48, is a reactive metal known for its diverse chemical properties. It readily forms compounds, reacts with oxygen to create cadmium oxide and exhibits variable solubility in water, typically in the  $\text{Cd}^{+2}$  oxidation state. Notably toxic, cadmium is used for corrosion resistance in plating applications, protecting metals in aerospace and automotive industries. With properties resembling zinc, it is malleable and ductile. In electrochemical applications, cadmium serves as an anode material in NiCd batteries. If adding the dual dopant material Cd to enhance the pure material properties and good efficiency of the devices. Due to toxicity, regulations restrict its use, prompting the search for alternative materials. K. Prasad as found as co doped with  $\text{Ce-CdO:Zn}$  [23].

There are various methods to form Ce-(Sn:Cd) thin films like JNSP, Sputtering, Spin Coating, laser ablation sputtering and six main types of

films are optical films, electronic films, magnetic films, chemical films, films and thermal films. Each type has different features areas of use so, no matter what application you need, there is a film to suit your needs and then the various techniques: Chemical Vapour Deposition, Plasma Enhanced Chemical Vapour Deposition, RF Magnetron sputtering, atomic layer deposition, Electrochemical method, Co-perception method sputtering, thermal evaporation, Carbon Coating, Electron Beam Evaporation, Molecular beam epitaxy, magnetron sputtering, sol-gel spin coating, spray pyrolysis, Jet Nebulizer Spray Pyrolysis [JNSP]. T. Lazar [24]. JNSP technology has numerous advantages such as cost effectiveness, modest test setup, high homogeneity, huge coverage area and product cleanliness. T. Alshahrani [25]. Moreover, the main challenge of JNSP technology is the control of film surface morphology, thickness and stoichiometry. A. Narmada [26]. V. Jagadeesan [27]. We can also adjust the discharge temperature, gas pressure and liquid volume throughout the film discharge process. J. Thangabalu [28]. The correction parameters of SBDs include the interface layer temperature. It is caused by the direct transfer of energy from high-energy materials to the lattice atoms in the spray field, which affects the performance of the device. In the JNSP technique the temperature is accompany to 450°C. Because only at this temperature can we obtain a good film with good performance and a clean film.

In present work Ce-(Sn:Cd) thin films were produced using JNSP technique for various wt% of Cd also persistent substrate temperature of 450 °C. Structural, morphological, optical & electrical properties of Ce-(Sn:Cd) analysed by XRD, AFM, UV-Vis, I-V characterizations. Also, the developed band gap of Ce-(Sn:Cd) thin films was employed as an interfacial layer (in between Cu/n-Si) in fabricating MIS structure SBDs. The novelty work we have taken using the dual doped material the cerium was band gap and also the doped Sn, Cd is less band gap is offering extra approaches with SBDs. The dual doped are using the diode fabrication the diode was overstated the electrical properties. Based on the varied light intensities, different Cd concentrations and the I-V characterization of the MIS structure diodes. The important diode parameters are n,  $\Phi_B$  and  $I_0$  are studied using J-V method and detail discussed below.

## 2. Experimental section

### 2.1. Pure Ce and dual doped Ce-(Sn:Cd) thin film preparation

Pure Ce, double-doped Ce-(Sn:Cd) films were prepared by dissolving 0.2 mol of cerium (III) chloride in 5 ml of ethanol and sonicating for 20 min. The solution stirred incessantly for 30 min using a magnetic stirrer under atmospheric conditions. Solutions were prepared using different concentrations of tin (II) chloride and cadmium chloride (V). Make it transparent, spray evenly and stir for another 20 min. The solution is sprayed onto clean glass using the JNSP process at the optimum substrate temperature (450°C). Parameter values are: nozzle radius 0.6 mm, distance between substrate and nozzle 8 cm, maintenance pressure 3.5 kg cm<sup>-2</sup>, flow rate 0.8 ml min<sup>-1</sup>, spraying time 15 min, spray gun type L quality and substrate temperature 450°C. Pure and doped solutions were chemically deposited on glass substrates heated at low temperatures and pure films were prepared.

### 2.2. Fabrication of MIS structure Schottky barrier diode

Cu/Ce-Sn: Cd/n-Si, MIS model diode made of n-Si wafer, target (100), thickness 279 ( $\pm 25$ )  $\mu\text{m}$ , ohmic resistance (0–60)  $\Omega \text{ cm}$ . Pure and different wt% Cd was used to produce SBDs with Cu/Ce-Sn: Cd/n-Si MIS structure. In this process, the bond solution is coated on an n-Si plate with dimensions of 1 cm  $\times$  1 cm. Before electroplating, n-Si sheets were cleaned with  $\text{H}_2\text{SO}_4 + \text{H}_2\text{O}_2$  solution (3:1). After the wafer is immersed in the colorful solution, it is placed in deionized water to remove unwanted impurity atoms. Also wash with (1:10)  $\text{H}_2\text{O} + \text{HF}$  solution to remove the oxide layer. Ce layer and double-doped Sn, Cd solution was

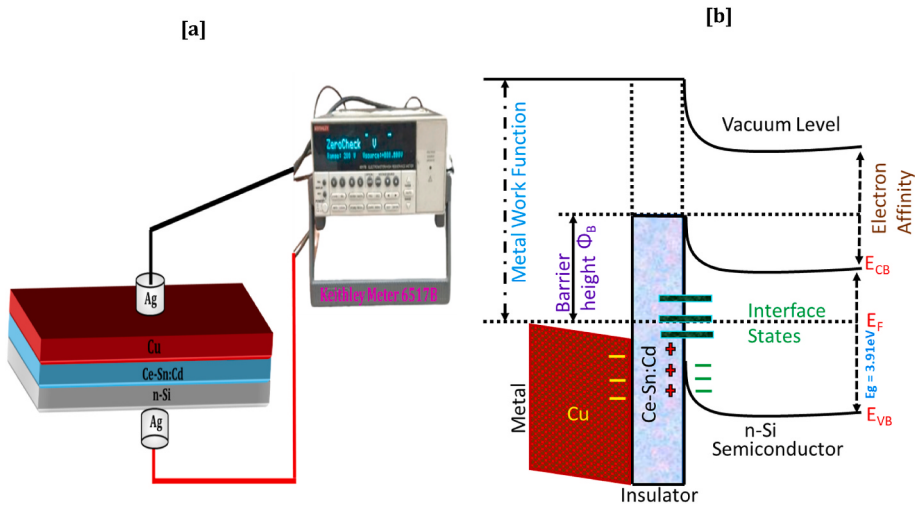


**Fig. 1.** [a] Schematic diagram for Ce–(Sn:Cd) fabricated with different Wt.% of Cd. [b] Energy level band diagram of the Cu/Ce–(Sn:Cd)/n-Si MIS interfacial layer.

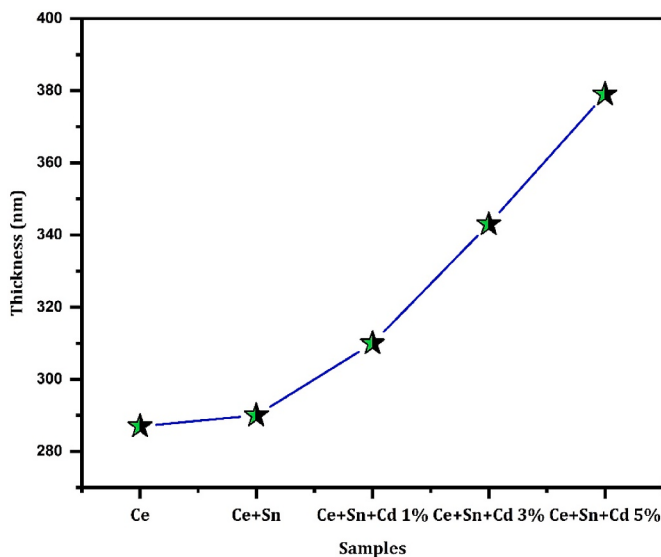


**Fig. 2.** Thickness variation of Ce–(Sn:Cd) thin films.

deposited on n-Si substrate at 450°C. Next comes the purification process, which removes impurities from the silicon substrate and obtains a pure substrate for production.

After the purification process, Ce–Sn and Ce–(Sn:Cd) solutions (3 ml) are sent to the bright environment and n-Si plate is produced using JNSP technology at 450 °C. Of these, DC magnetron sputtering is used. Transfer high purity metal (Cu) or transfer metal (4 mm diameter) onto Ce–Sn and Ce–(Sn:Cd) films. The deposition parameters of the Cu contact are fixed after many trials as pressure = 6 mbar, thickness = 500 nm. Additionally, forged SBDs of the MIS structure was used to analyze I–V characteristics for optoelectronic applications. A. Baltakesmez [29]. Silver paste is used to form ohmic contact between the rough surface of the n-Si substrate and the contact front of the metal material then dried at room temperature for 4 h. Remove the iron and add isoamyl acetate. Use a brush to mix while painting. When you apply the same layer, after a few minutes the isoamyl acetate will evaporate and you will get the real silver color. Silver paste is used to produce copper according to MIS standards. Fig. 1(a) shows the schematic diagram of the Cu/Ce–(Sn:Cd)/n-Si material. Fig. 1(b) In the present work Ce–(Sn:Cd) act as an insulator layer blocking the free states at the MIS interface. In this work. Therefore, it gradually increases the effective  $\Phi_B$  of the Schottky device

with Cu/Ce–(Sn:Cd)/n-Si MIS structure.

### 2.3. Characterization techniques

The deposited films were examined according to XRD, AFM, UV–vis and I–V properties. Structural defects of Ce, Ce–Sn and Ce–(Sn:Cd) films were measured using an X-ray diffractometer (Rigaku Miniflex-II) with electron source  $\text{CuK}\alpha 1$  ( $\lambda = 1.5418 \text{ \AA}$ ). The surface roughness of the secreted films was measured using atomic force microscopy (AFM). Optical properties of Ce–(Sn:Cd) films were obtained with a UV–visible spectrophotometer (JASCO UV–vis, model V–770 P C). The negative conductivities of Ce–(Sn:Cd) films and Cu/Ce–(Sn:Cd)/n-Si structured diodes were determined with Keithley's field tester (Model 6517-B). Additionally, the critical forward and reverse current of the MIS diode were measured using a solar simulator (PEC-L01) under different illumination conditions.

## 3. Results and discussion

### 3.1. Measurement of sample thickness

Got the information about the thickness of the film by measuring the thickness of the film with a Stylus profilometer. The thin film produced by spray pyrolysis is greatly affected by the solution, substrate treatment and control of spray time. Fig. 2 shows the film thicknesses of 287, 290, 310, 343 and 379 nm for pure Ce and 1, 3 and 5 wt% dopants. As the additive concentration increases, the film thickness increases. As the doping concentration increases, more dopant atoms fill the defects. The additive concentration increases and forms a new microcrystalline orientation layer, thus increasing the film thickness.

### 3.2. Structural scrutiny

Fig. 3 appearance the X-ray diffraction patterns of the Ce–(Sn:Cd) thin films capped at different concentration (1, 3 and 5 wt%). The thin films capped at constant substrate temperature of 450°C. Then the structural parameters and phase recognition are put through using an Ultima 3 Rigaku X-ray diffract meter at scanning rate of  $0.2\text{min}^{-1}$  in the range between 10 and 80. The diffraction position at 20 values is 29.31, 33.31, 47.80, 56.80, 59.56, 69.96 and 76.81 and similar miller indices (hkl) values are 200, 222, 400, 440 and 622 are sustained approve cubic structure. The identified peak values are associated with (JCPDS = 48–0641). Illustrates that the observed peak 222 position has aged towards lower angle  $2\theta = 29.3$  to 28.5 when Cd concentration is increased. Other orientations with low relative intensities when collate to the 222

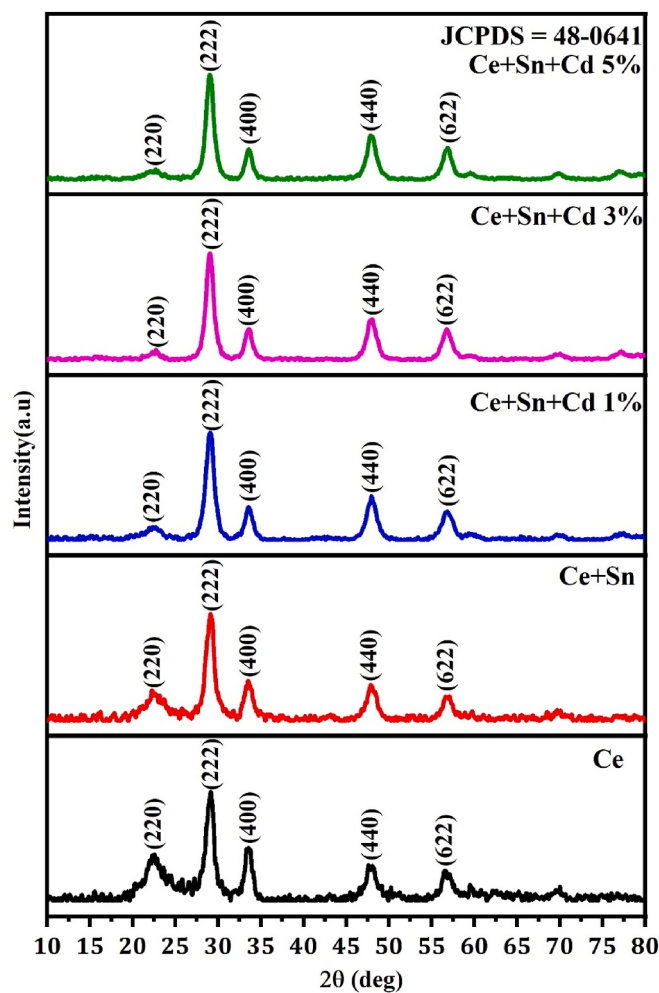


**Fig. 3.** XRD pattern shows that the Ce-(Sn:Cd) films for variation of Cd.

directions include 220, 400, 440 and 622. It confirms to the crystalline growing in the 222-plane direction. Improving the crystalline quality of the films. Owing to substantiate that the crystalline growth along 222 directions with upgraded crystalline nature of the Ce-(Sn:Cd) thin films also diminish the intensity peaks and enlarge the crystalline size. The

crystalline parameters deliberate Ce and are for list in **Table 1**. Obviously, a Crystalline size (D) of the thin films were found to enlarge gradually with lofty Cd concentration (1, 3 and 5 wt%). The crystalline size (D) of pure Ce thin film was 18.26 nm, which enlarge to 24.89 nm on increasing the Cd concentration from (1, 3 and 5 wt%). P. Vivek as same as increased the crystalline size [30]. And the order of increase is the same as the instructions in the previous work [31–35]. This is because we obtained the minimum filtration and dislocation rate values for high Cd concentration (5 wt%). In particular, the crystal size of 5 wt% Cd is 24.89 nm. This size indicates that there are more nucleation sites, more sintering flux and other factors can also increase the size of crystallinity by heat treatment at the substrate temperature (450°C) [36]. The average crystal size is calculated from the full width at half maximum of the XRD line using the Debye Scherer formula [37].

$$D = \frac{k\lambda}{\beta \cos \theta} \quad (1)$$

Here, K- ( $k = 0.94$ ) constant value,  $\lambda$ -wavelength in angstrom,  $\theta$ - Bragg's angle and  $\beta$ -line width at half maximum.

The Micro-Strain  $\varepsilon$ , Dislocation density  $\delta$  and Stacking Fault SF of hidden Ce-(Sn:Cd) thin films were deliberate using the following. Equations [2–4].

$$\varepsilon = \beta \frac{\cos \theta}{4} \quad (2)$$

$$\delta = \frac{1}{D^2} \quad (3)$$

$$SF = \left[ \frac{2\pi^2}{45(3 \tan \theta)^{\frac{1}{2}}} \right] \beta \quad (4)$$

The deliberate structural parameter is Micro-Strain  $\varepsilon$ , Dislocation density  $\delta$  and Stacking Fault SF with dissimilar doped concentration (1, 3 and 5 wt%). The thoughtful crystalline parameters for thin films increase Cd concentration when compare to pure films, to the control of Ce-Sn and Ce-(Sn:Cd) lattices. Because of annihilation of lattice defects with increasing in the doped concentration, the strain, besides the lattice and dislocation density in the films, elevated average value of micro-strain is 0.1642. We observed the preferential orientation along the (222) plane of pure Ce, dual doped Ce-Sn and Ce-(Sn:Cd) for lofty concentration of 5 wt% Cd. This result suggest that the Cd concentration resolutely varies the favour inclination of Ce-Sn and Ce-(Sn:Cd) crystal planes. Principally, dislocation density value ( $3.00\text{--}3.75 \times 10^{15}$  lines/ $\text{m}^{-2}$ )

**Table 1**  
Calculated structural parameters of Ce-(Sn:Cd) thin films for various wt%.

Sample code	Diffraction angle 2θ (deg)	(hkl) values	Inter planar distance d (Å)	FWHM Radians	Crystallite size (D) (nm)	Micro strain ( $\varepsilon \times 10^{-3}$ lines $^{-2} \text{m}^{-4}$ )	Dislocation density ( $\delta \times 10^{15}$ lines $\text{m}^{-2}$ )	stacking fault (SF x $10^{-2}$ )
Ce	29.1985	222	3.0585	0.8029	17.85	0.1942	3.1352	0.4559
	33.5188	400	2.6735	0.8029	18.04	0.1921	3.0691	0.4964
	47.8870	440	1.8996	0.8029	18.90	0.1834	2.7965	0.6415
Ce+Sn	29.3034	222	3.0478	0.4684	30.62	0.1132	1.0665	0.2665
	33.6381	400	2.6643	0.9368	15.47	0.2241	4.1762	0.5805
	47.8222	440	1.9020	0.6691	22.68	0.1529	1.9431	0.5340
Ce+Sn+Cd 1%	57.1502	622	1.6117	0.9368	16.86	0.2056	3.5151	0.8856
	29.2291	222	3.0554	0.5353	26.78	0.1294	1.3934	0.3042
	33.6079	400	2.666	0.4684	30.94	0.1121	1.0442	0.2900
Ce+Sn+Cd 3%	56.6877	622	1.6238	0.8029	19.63	0.1766	2.5933	0.7524
	22.6086	220	3.9329	0.8029	17.62	0.1968	3.2193	0.3936
	29.1001	222	3.0687	0.6691	21.42	0.1619	2.1783	0.3792
Ce+Sn+Cd 5%	33.7061	400	2.6591	0.7360	19.69	0.1760	2.5768	0.4566
	56.8386	622	1.6198	0.5353	29.47	0.1176	1.1511	0.5030
	29.2400	222	3.0542	0.8029	17.86	0.1942	3.1346	0.4563
	33.5546	400	2.6708	0.6691	27.07	0.1281	1.3641	0.3311
	47.8041	440	1.9027	0.7360	37.80	0.0917	6.9976	0.3203
	56.8036	622	1.6208	0.5353	16.83	0.2060	3.5266	0.8798

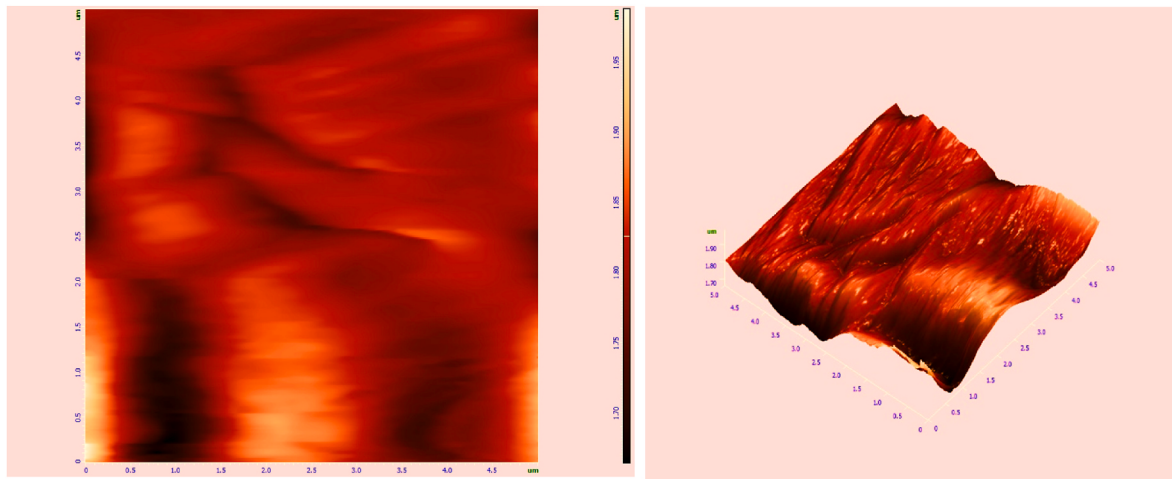


**Fig. 4.** AFM Topography view of 5 wt% Ce-(Sn:Cd) thin films.

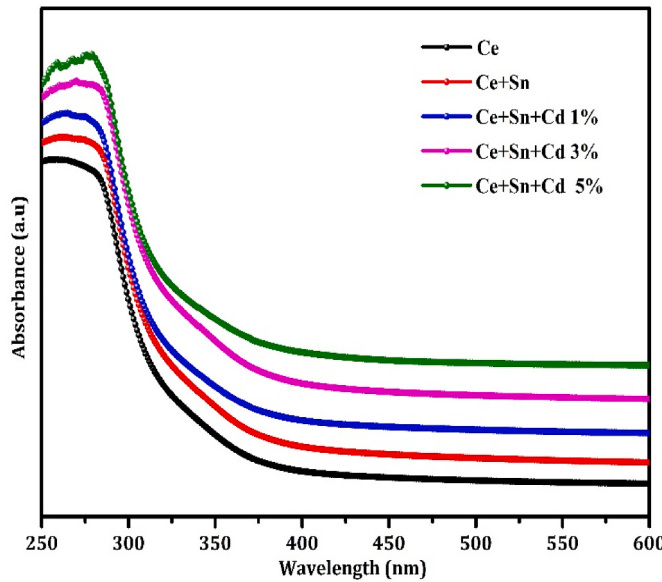


**Fig. 5.** Absorption spectrum Ce-(Sn:Cd) films with different wt% of Cd.

**Table 2**  
Optical parameters of Ce-(Sn:Cd) films.

Sample code	Absorption coefficient ( $\alpha \times 10^7$ (cm) $^{-1}$ )	Extinction coefficient (k)	Optical band gap (Eg) (eV)	Optical conductivity ( $\sigma_{\text{opt}}$ ) (S/cm)
Ce+Sn	2.4814	0.1854	3.97	$1.34 \times 10^{14}$
Ce+Sn+Cd 1%	2.5910	0.2743	3.93	$2.93 \times 10^{14}$
Ce+Sn+Cd 3%	2.6812	0.3832	3.88	$5.71 \times 10^{14}$
Ce+Sn+Cd 5%	2.8800	0.4849	3.85	$9.15 \times 10^{14}$

$m^2$ ) of thin films diminished with increasing Cd concentration. Since dislocation velocity represents the collection of dislocations in the film, an increase in dislocation velocity indicates the creation of a better film [38]. The films with 5 wt% of Cd let out lofty average value of micro-strain and stacking fault ( $0.53$  and  $0.49 \times 10^{-2}$ ). Due to this may have something to do with the film's ability to relieve stress [39]. Owing, to thin films with good crystalline properties will have low contrast and significant MIS values [40,41]. In this case, the calculated

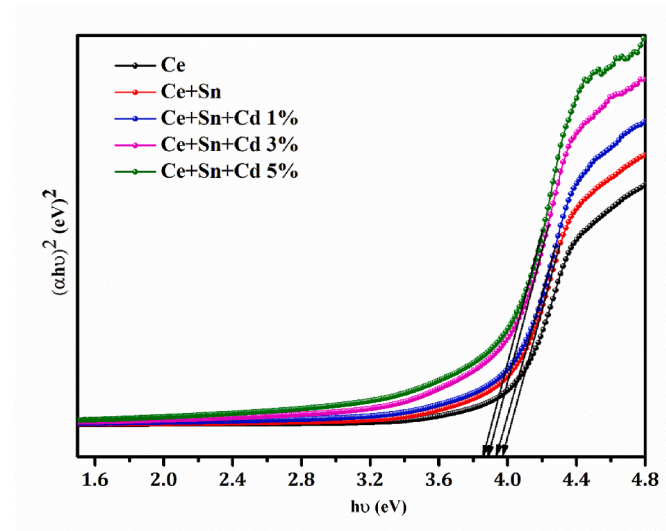


**Fig. 6.** Plot of  $(\alpha h\nu)^2$  (eV) $^2$  vs  $h\nu$  (eV) for the Ce-(Sn:Cd) films.

dislocation speed and MIS values decrease with increasing doping concentration, which causes crystal defects to change [42]. Owing to optimized temperature, the defects in the Ce-(Sn:Cd) lattice regions disappear and the gap between the film's changes [43]. The maximum dual doped concentration of Ce-Sn and Ce-(Sn:Cd) uncover the better result while collate with other wt%. From the results, we can see those small changes in the Ce-(Sn:Cd) films deliberately improve the crystal properties and increase the efficiency of Ce-(Sn:Cd) thin films. As the Cd dopant concentration increases, lattice defects are eliminated and the MIS structure appears to enhance photodiode properties of the diode [36].

### 3.3. Investigation of AFM - surface roughness analysis

AFM depicts of Ce-(Sn:Cd) with 5 wt% contractions when demonstrated in Fig. 4 AFM depicts of the surface of thin films when they underwent scanning at  $10 \mu\text{m} \times 10 \mu\text{m}$  areas afford an illustration of the surface morphology of the structure. AFM portrait is usually utilized to convey the surface morphology learning of hidden thin film, which is beneficial for evaluating the type of grains and surface roughness. Relation is having been utilized to find the Root Mean Square (RMS) roughness mean.

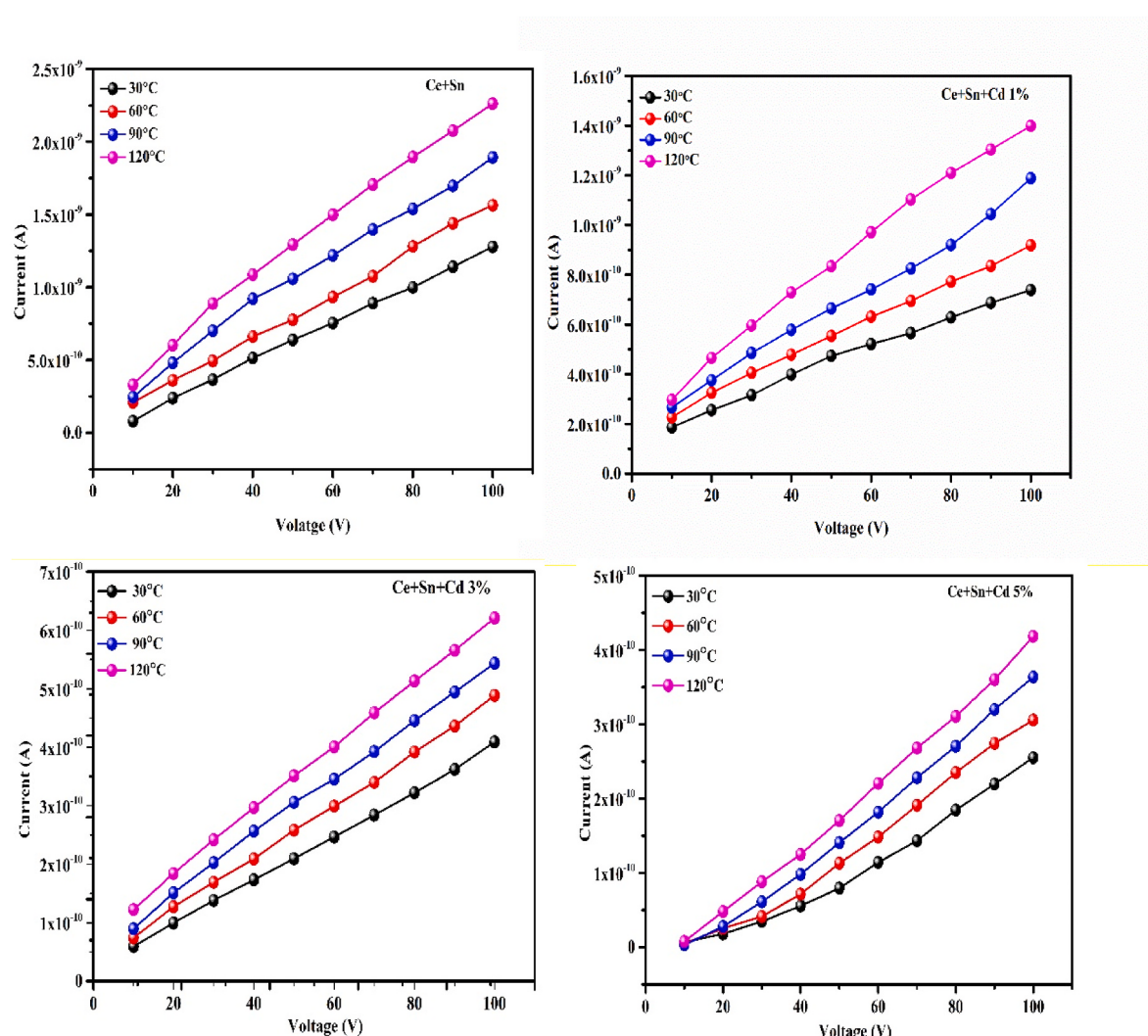


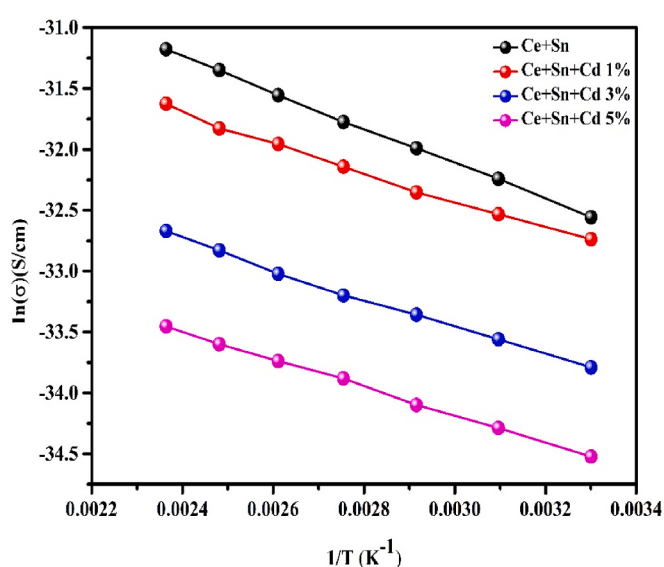
Fig. 7. I-V characteristics of Ce-(Sn:Cd) films for different wt% of Cd.

**Table 3**  
Electrical Parameters of  $\rho$ ,  $\sigma_{dc}$  and  $E_a$  for films.

Sample code	Resistivity ( $\rho$ ) ( $\Omega \cdot \text{cm}$ )	Electrical conductivity ( $\sigma_{dc}$ ) (S/cm)	Activation Energy ( $E_a$ ) (eV)
Ce+sn	$9.6 \times 10^{-13}$	$1.7 \times 10^{-14}$	0.0943
Ce+Sn+Cd 1%	$1.1 \times 10^{-14}$	$1.1 \times 10^{-14}$	0.0760
Ce+Sn+Cd 3%	$2.5 \times 10^{-14}$	$1.9 \times 10^{-15}$	0.0701
Ce+Sn+Cd 5%	$6.8 \times 10^{-14}$	$4.0 \times 10^{-15}$	0.0673

$$\text{RMS} = \sqrt{\frac{1}{N} \sum_{i=1}^N Z_i^2} \quad (5)$$

$N$ - total number of pixels detected,  $Z_i$  - height difference with respect to the average height of the film surface. The surface of the Ce-(Sn:Cd) thin films is equitably smooth, as demonstrated based on derived RMS value of 23.86 nm. This sort of roughness reduce is correlates with variation in crystallite size, which was demonstrated by an XRD research. The emergence of a consistent layer of Ce-(Sn:Cd) on n-Si surface is acceptable for device manufacturing, pursuant to the pretty smooth surface roughness value of 17.51 nm. The increase in roughness

Fig. 8. Arrhenius plots of  $1/T$  ( $K^{-1}$ ) vs  $\ln(\sigma)$  (S/cm) for Ce-(Sn:Cd) films.

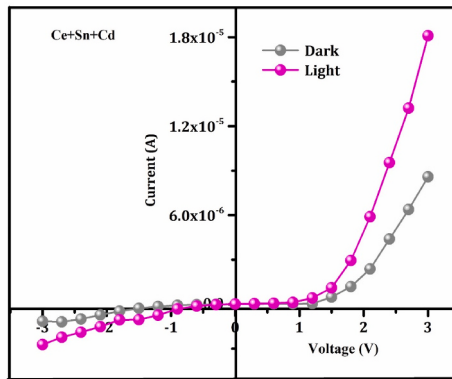
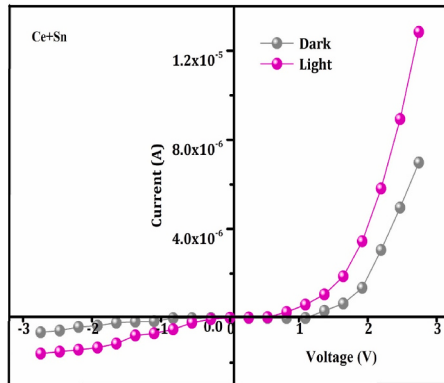


**Fig. 9.** I-V characteristics for Ce-(Sn:Cd) MIS structure with Cd wt%.

can be attributed to the reaction separation and deformation as well as the deformation pattern of the film itself [44]. By changing JNSP technique parameters such coating time, RPM/mints, the volume of solution among others, it is simple to manipulating the thin film's 102.156 nm thickness. The results presented by Pan et al. showed similar results for cerium and tin doped Cd [45]. It can also be seen that the surface is further processed, so that the gaps between the grains become smaller and even merge or disappear into a thin film, which helps reduce the water flow current and dielectric loss [46,47]. When Ce-Sn is double-doped with Cd, the resistance of the thin film increases with the Cd content of the growth solution. These findings contribute to the Schottky device's improved rectification nature and overstated photo diode property when collate to other works.

#### 3.4. UV-visible spectroscopy

We have used UV-Vis's spectroscopy to analyze the optical characteristics of Cd doped films in order to further examine the capped thin films. In the applications of optoelectronic devices, the optical characteristics of thin films, such as absorbance & band gap, are extremely important.

##### 3.4.1. Absorbance(A)

Fig. 5 represents the absorbance spectra of thin films with dual doped of Ce-Sn and Ce-(Sn:Cd) for wavelengths around 250 and 600 nm. Because of the rise in thin film thickness, the absorbance of the films has increased with Cd content (1, 3 and 5 wt%). Ce thin films have a cut-off

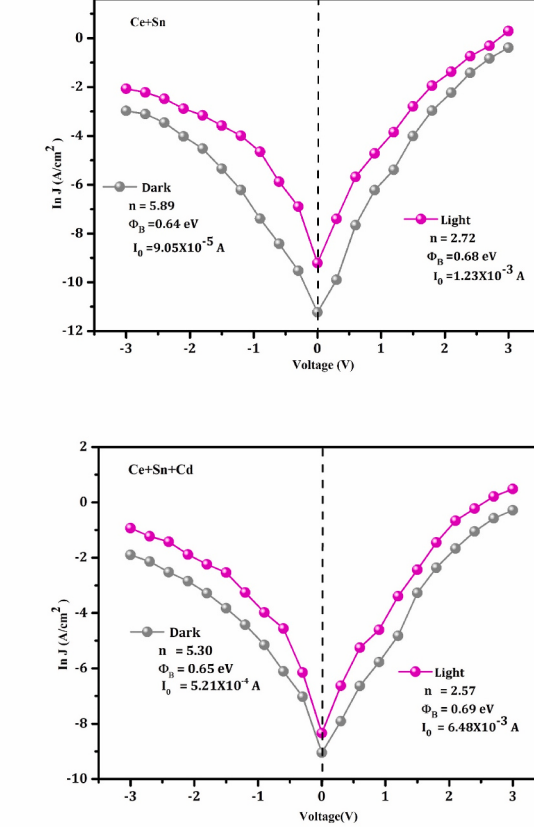


**Fig. 10.** Semi-logarithmic plot of current vs voltage for Cu/Ce-(Sn:Cd)/n-Si MIS structure diode.

**Table 4**

Ideal parameters of n,  $\Phi_B$ ,  $I_0$  Cu/Ce-Sn:Cd/n-Si MIS structure diode.

Sample Code	Condition	Ideality Factor (n)	Barrier Height ( $\Phi_B$ ) eV	Saturation Current ( $I_0$ )
<b>Ce+sn</b>	Dark	5.89	0.64	$9.05 \times 10^{-5}$
	Light	2.72	0.68	$1.23 \times 10^{-3}$
<b>Ce+Sn+Cd</b> 5%	Dark	5.30	0.65	$5.21 \times 10^{-4}$
	Light	2.57	0.69	$6.48 \times 10^{-3}$

wavelength of about 270 nm and this edge revealed the produced film's high crystalline quality. Table 2 lists the optical characteristics, absorbance and Cd doped concentration. Both pure Ce and dual doped of Ce-Sn, Ce-(Sn:Cd) thin films exhibit almost constant UV-visible absorption. Since, there is an inverse relationship between transmission and absorption [48]. Additionally, films exhibit undeniable dampening as a result of the large density and thickness of free electrons. Because the higher absorption film can generate the light in the photodiode material and thus improve the role of the diode [49]. Due to the abundance of free electrons, the observed absorbance clearly demonstrates dampening and its large crystalline size and smooth surface [50,51]. Which are relatively greater than those of other Ce thin films, 5 wt% of Ce dual doped Sn, Cd thin film as validated by XRD and AFM pictures separately, exhibits the greatest absorbance. Furthermore, a thin film with a loft absorbance will be ideal for industrial photovoltaic uses, particularly as a photo diode. It's because thin films with the higher absorption may carry out as good light armour in MIS device under illumination condition which will in enhance the reactive of diode along with the ascendancy of photogenerated charge carriers it is more

**Table 5**

Comparison of the Cu/Ce-(Sn:Cd)/n-Si diode performance with previous reports.

S. No	Author name	Technique	Diode Structure	Ideality factor (n)	Barrier Height $\Phi_B$ (eV)	Ref
1	P. Vivek et al.,	Jet Nebulizer Spray Pyrolysis (JNSP)	Cu/MoO <sub>3</sub> -ZrO <sub>2</sub> /p-Si	2.98	0.63	[85]
2	R. Marnadu et al.,	JNSP	Cu/nano porous: Cu/Sr-Wo <sub>3</sub> /p-Si	2.78	0.63	[33]
3	R. Marnadu et al.,	JNSP	Cu/Sr-Wo <sub>3</sub> /p-Si	3.91	0.54	[86]
4	P. Vivek et al.,	JNSP	Cu/Ga-MoO <sub>3</sub> /p-Si	3.07	0.68	[37]
5	P. Vidhya et al.,	JNSP	P-Pbs/n-Si	4.47	0.64	[87]
6	K.S. Mohan et al.,	JNSP	n-Yb <sub>2</sub> O <sub>3</sub> /p-Si	2.94	0.66	[88]
7	P. Vidhya et al.,	JNSP	Ce-pbs/n-Si	3.82	0.68	[43]
8	M. Justin Paul et al.,	Co – Precipitation	P-CuO/n-Si	4.69	0.52	[89]
9	S. Kalidass et al.,	JNSP	n-AlZnO/p-Si	3.69	–	[90]
11	Ahmet Kaymaz et al.,	Sol gel spin coating	Al/(ZnO-PVA) p-Si	6.37	0.57	[91]
12	R. Marnadu et al.,	JNSP	Cu/WO <sub>3</sub> -nanoplates/p-Si	4.89	0.64	[92]
13	V. Balasubramani et al.,	Sol gel spin coating	Cu/V <sub>2</sub> O <sub>5</sub> /n-Si	5.26	0.46	[40]
14	M. Balaji et al.,	JNSP	p-Si/n-MO <sub>3</sub>	5.99	0.51	[93]
15	Present work	JNSP	Cu/Ce-Sn:Cd/n-Si	2.57	0.69	–

applicable for optoelectronics.

### 3.4.2. Optical energy gap ( $E_g$ )

Fig. 6 represents the optical energy gap values of Ce dual doped Ce-Sn and Ce-(Sn:Cd) thin films. By employing the flowing relation and an extension of a straight line in Taue's figure, the band gap values are computed.

$$(\alpha h\nu)^n = B(h\nu - E_g) \quad (6)$$

Of these,  $n = 2$  - direct variation,  $\alpha$  - absorption coefficient,  $h\nu$  - incident photon energy,  $B$  - constant and  $E$  – light band energy of the sample film. The change in optical properties of pure Ce-Sn, Ce-(Sn:Cd) films and double-doped Ce-Sn films. The optical band gap values obtained from the graphs were found to be 3.97, 3.93, 3.88 and 3.85 eV, respectively, according to the concentration varied band gaps of Cd doped (1, 3 and 5 wt%). This is because new defects are formed as gas defects form around the Fermi level. Hence, excess electrons near the conduction band (CB) will enter the lower side of the gap [52,53]. Structural change confirmed by XRD favour is the reason to decrease in band gap values at optimized substrate temperature. Moreover, the decrease in  $E_g$  is due to the addition of Ce-Sn to the Ce-(Sn:Cd) doping, which creates an energy pollution in the matrix below the conduction band and also causes sp-d interaction with tungsten ions [54,55]. As the Cd concentration increases, planar defects form with the incorporation of new atoms, stacking and grain boundaries are disrupted [56]. We also measured the important optical parameters like absorption co-efficient ( $\alpha$ ), extinction coefficient ( $\kappa$ ) using the following relation:

$$\alpha = \left( \frac{1}{d} \right) \ln \left( \frac{1}{T} \right) \quad (7)$$

$$\kappa = \frac{\alpha \lambda}{4\pi} \quad (8)$$

Of these,  $T$  - permittivity,  $d$  - thickness of the film,  $\alpha$  - absorption coefficient and  $\kappa$  - extinction coefficient. The average absorption coefficient is  $2.65 \times 10^7$  (cm)<sup>-1</sup>, extinction coefficient is 0.332 and optical density is  $4.78 \times 10^{14}$  as the result increases because of the extra photon energy is absorbed by free electrons entering the layer [57]. In addition, loss and breakage of the lens will affect the extinction coefficient of the film [58]. Band gap ( $E_g$ ) of 5 wt% Ce-(Sn:Cd) thin film is remarkably less than that of other Ce thin film. Ce-Sn and Ce-(Sn:Cd) thin films with dual doped may have distinct band gap values because of the following factors: An enlarge in film thickness and a density of localized states close to the band boundaries. Thus, the effective optical  $E_g$  reduces as a result of doped as the band pursuit or debasement band widens and eventually approaches to combine at the radical of the conduction band. Moreover, the Cd concentration dopant extra influence, including the impact of their 4f-electrons on the crystalline electronic states, results in a change

in the type and intensity of the crystalline potential, which in turn causes the band gap to reduce [59]. The band gap energy of pure Ce is lofty than the dual doped Ce-(Sn:Cd) thin films overdue to Cd concentration, which make an energy level near to the valence band employed by the electrons.

### 3.5. Electrical property

#### 3.5.1. Electrical conductivity (DC)

The electrical conductivity (DC) of the films was measured with a Keithley electrometer equipped with two probes. A constant voltage of 10–100 V was implemented and electrical conductivity was sustained at 30°C intervals for temperatures fluctuating from ambient temperature to 120°C using a controlled oven. Fig. 7 depicts the I-V characteristics of Ce and dual dopant Ce-(Sn:Cd) thin films with concentrations of (1, 3 and 5 wt%). The calculated values of the electrical conductivity ( $\sigma_{dc}$ ) and activation energy ( $E_a$ ) of the films produced were intentionally constructed using the following relationships. The following equation can be employed to calculating the electrical conductivity.

$$\sigma_{dc} = \left( \frac{I}{V} \right) \times \left( \frac{d}{A} \right) S / \text{cm} \quad (9)$$

It is determined by the output current  $I$ , the power consumption  $V$ , the distance  $d$  between the two probes and the Cross-section  $A$ . Required conductivity, resistance and activation energy values are listed in Table 3. It was found that the required area change with different Cd varies between electrical conductivity ( $1.7 \times 10^{-14}$  and  $4.06 \times 10^{-15}$  S/cm). Since thermally activated chargers can easily jump from one place to another at higher temperature [60]. This is ideal for improving the rectifying behaviour of diodes based on MIS standards [61]. In addition, changes in optical properties (decreasing band gap values) with increasing concentration are associated with changes in conductivity [62]. It is clear that the resistivity ( $9.6 \times 10^{-13}$  to  $6.8 \times 10^{-14}$  Ω cm) increases Cd concentration (1, 3 and 5 wt%). Moreover, the higher the film thickness obtained, the crystallite size of the film can be improved, which reduces the impact and hence a small amount of electricity will be trapped in the grain and a large number of electrons can participate in DC conduction [63]. Fig. 8, it is clearly seen that Cd with higher wt% in the doped film shows better conductivity than Cd with lower wt%. The obtained  $\sigma_{dc}$  value is suitable for the design of MIS type Schottky components. Activation energy  $E_a$  is the minimum energy required to open the atomic structure of the thin film and is deliberately calculated according to the following equation.

$$E_a = \text{slope value} \times \left( \frac{K_B}{e} \right) \text{ eV} \quad (10)$$

Of these,  $K_B$  - Boltzmann constant and  $e$  – electric charge. The functional energy of the Ce-(Sn:Cd) latent thin film varies from 0.09 to

0.06 eV with Cd dopant concentration (1, 3 and 5 wt%). Due to this behaviour can be achieved in Ce-(Sn:Cd) films, as thermally activated electrons are transferred from VB to CB without traps and defects [64]. It is worth noting that when the amount of Cd additive is 5% by weight, the activation energy of the Ce-(Sn:Cd) film is the lowest and its electrical conductivity is the highest. In addition, the film's flat structure, limited crystal defects and improved optical properties can improve MIS-type photodiode performance compared to other Cd doping concentrations. The addition of Cd concentrations significantly increases the electrical behaviour of Ce-(Sn:Cd) thin films. Due to this can be understood as the effect of load loading due to boundary deformation [65]. It is attributed to the lofty crystalline quality of the film as confirmed by XRD analysis.

### 3.5.2. Schottky barrier diode of Cu/Ce-(Sn: Cd)/n-Si MIS structure

Current-voltage (I-V) measurements in dark, light conditions investigate the properties of the photodiode and the performance of Schottky barrier diodes. The thickness of the interface layer of MIS-type diodes also plays a dual role: it is translucent to the energy of electrons from the metal to the semiconductor, which clarifies the conditions for how much the minority carrier injects and blocks current. C. S. Guclu [66]. This special feature prevents high leakage current, which cannot be found in MS SBDs contacts. Photo diode performance of Cu/Ce-(Sn: Cd)/n-Si, MIS structured diodes. Fig. 9 shows the measured I-V properties of Cu/Ce-(Sn:Cd)/n-Si SBDs with double-doped Ce-Sn and Ce-(Sn: Cd) based insulating layer in light and dark illuminations. S. O. Tan [67]. The dark current, photocurrent of the MIS diodes were measured with a Keithley electrometer measuring a negative contact from -3 to +3v. Also, Cu/Ce-(Sn:Cd)/n-Si SBDs measurements were examined under halogen light and dark conditions. Therefore, as the interface layer or average barrier thickness decreases, the current increases [68]. The Current conduction implementations of the Cu/Ce-(Sn:Cd)/n-Si diode have been described using the following relationship [11,12].

$$I = I_0 [\exp(q(V - IR_s)/nK_B T) - 1] \quad (11)$$

$$I_0 = AA^*T^2 \exp(-q\phi_B/K_B T) \quad (12)$$

Of these, Saturation Current ( $I_0$ ), Electron Charge (q), Bias voltage (V), Ideality factor (n), Positive barrier height ( $\Phi_B$ ), Boltzmann constant ( $K_B$ ) and temperature (T). Comparing dark and light conditions, all MIS diodes performed well in bright light. The diode (n) is determined by interpolating the value of the measured voltage distribution (v), as shown in Fig. 10. It is worth noting that the input value of the (n) diode decreases linearly with increasing xenon light. Interestingly, many research groups have also observed similar behaviour for different types of construction equipment using various types of deposits [69–74]. The (n) and ( $\Phi_B$ ) have a significant impact on its performance, which can be attributed to the following relationship [13,14].

$$\text{Ideality factor (n)} = \frac{q}{K_B T} \frac{dV}{d(\ln I)} \quad (13)$$

$$\text{barrier height } (\phi_B) = \frac{K_B T}{q} \ln \left( \frac{AA^*T^2}{I_0} \right) \quad (14)$$

The fabricated Schottky MIS structured diode demonstrates (n) between 5.89 and 2.57 is not equal to one. If n equals one, diode produces untainted thermionic emission however, n is typically greater than unity. Another reason for the higher efficiency of the Cu/Ce-(Sn:Cd)/n-Si, MIS junction may be owing to the competitive nature of the metal-induced state difference and bias of ( $\Phi_B$ ) [75]. This may occur due to rearrangement of electron-hole pairs under illumination conditions [40]. Upon dual doped Ce-Sn and Ce-(Sn:Cd) n reduces and  $\Phi_B$  increases as portrayed in Table 4. It suggests the concentration of a doped substance alters the electrical properties of the diode, thereby enhancing its performance. Moreover, the charges in the semiconductor band flexed because of interactions between metallic layer and the changed

substrate may have the disparity in barrier height. E. E. Tanrikulu [76]. These centres prevent the free flow of charge carriers and increase the barrier height causing shrinking [77]. The results show that the addition of doped ions forms chemically induced interlayers, leading to a decrease in the (n), an increase in the ( $\Phi_B$ ) and decrease in the Saturation Current ( $I_0$ ). Ce-Sn and Ce-(Sn:Cd) produce high luminous intensity (I-V) with good illumination (n = 2.57),  $\Phi_B$  value of 0.69 eV and saturation ( $I_0$ ) of  $6.48 \times 10^{-3}$  A. E. E. Tanrikulu [78]. Defects isolated at the boundary can disrupt carriers and restore current density by providing a glide path for transport [79,80]. This can be attributed to the formation of a small number of ( $e^-h^+$ ) pairs and their recombination. P. Harish Senthil [81]. Correlations are then analysed to obtain more features Table 5. H. Elamen [82]. M. A. Salari et al., [83]. This study compares the performance of Cu/Ce-(Sn:Cd)/n-Si diodes with previous reports. V. Balasubramani [84]. The results of this study support the same proposition regarding height measurement as compared with the previous study we found that the JNSP is the best technique and we got the better barrier height and ideality factor.

## 4. Conclusion

Dual doped Ce-(Sn:Cd) thin films with different Cd concentrations and Cu/Ce-(Sn:Cd)/n-Si structured Schottky diode was successfully fabricated by JNSP techniques. According to structural study, the crystallite size increased 18.26 nm–24.89 nm. Additionally, a cubic crystal structure without any phase transitions was seen in the XRD pattern then the value of the Cd film surface roughness is reduced by the incorporation of Ce ions. At 5 wt percent, the lowest roughness value of 17.51 nm was measured. The higher Cd concentration of 5 wt% in the UV-Vis study showed maximal optical absorbance with a smaller band gap of 3.85 eV. The Cu/Ce-(Sn:Cd)/n-Si diode performed better than other diodes under light conditions, according to its I-V characteristics. The 5 wt% diode attained an impressive (n) of 2.57,  $\Phi_B = 0.69$  eV for the barrier height and  $I_0 = 6.48 \times 10^{-3}$  A for the saturation current. Our findings executed that the Ce-(Sn:Cd) thin films, makes an improved interfacial layer for Schottky diodes and photovoltaic changes, manufacturing it appropriated for more suitable for photodiode applications.

## Funding

Funding associate in this work.

## Data availability statement

Data is available on request.

## CRediT authorship contribution statement

**T. Akila:** Writing – original draft, Data curation. **P. Gayathri:** Writing – review & editing. **G. Alan Sibu:** Writing – review & editing. **V. Balasubramani:** Writing – review & editing, Supervision. **Hamad Al-lohedan:** Writing – review & editing. **Dhaifallah M. Al-dhayani:** Writing – review & editing.

## Declaration of competing interest

The authors declare that they have no known competing financial interests or personal relationships that could have appeared to influence the work reported in this study.

## Data availability

No data was used for the research described in the article.

## Acknowledgements

The authors extend their appreciation for funding to Researchers Supporting Project number (RSP2024R54), King Saud University, Riyadh, Saudi Arabia.

## References

- [1] R. Marnadu, J. Chandrasekaran, S. Maruthamuthu, V. Balasubramani, P. Vivek, R. Suresh, Ultra-high photo response with superiorly sensitive metal-insulator-semiconductor (MIS) structured diodes for UV photodetector application, *Appl. Surf. Sci.* 480 (2019) 308–322.
- [2] M. Soylu, F. Yakuphanoglu, Photovoltaic and interface state density properties of the Au/n-GaAs Schottky barrier solar cell, *Thin Solid Films* 519 (2011) 1950–1954.
- [3] M. Ali, V. Cimalla, V. Lebedev, H. Romanus, V. Tilak, D. Merfeld, P. Sandvik, O. Ambacher, Pt/GaN Schottky diodes for hydrogen gas sensors, *Sensor. Actuator. B Chem.* 113 (2006) 797–804.
- [4] P.C. Chang, Y.K. Su, K.J. Lee, C.L. Yu, S.J. Chang, C.H. Liu, Improved performance of GaN-based Schottky barrier photodetectors by annealing Ir/Pt Schottky contact in O<sub>2</sub>, *J. Alloys Compd.* 504 (2010) S429–S431.
- [5] A. Maestrini, B. Thomas, H. Wang, C. Jung, J. Treuttel, Y. Jin, G. Chattopadhyay, I. Mehdi, G. Beaudin, Schottky diode-based terahertz frequency multipliers and mixers, *Compt. Rendus Phys.* 11 (2010) 480–495.
- [6] N. Başman, O. Uzun, S. Fiat, C. Alkan, G. Cankaya, Electrical characterization of a pre-ceramic polymer modified Ag/poly (hydrido carbyne)/p-Si Schottky barrier diode, *J. Mater. Sci. Mater. Electron.* 23 (2012) 2282–2288.
- [7] H. Jeong, H.M. Oh, S. Bang, H.J. Jeong, S.J. An, G.H. Han, H. Kim, Metal-insulator-semiconductor diode consisting of two-dimensional nanomaterials, *Nano Lett.* 16 (2016) 1858–1862.
- [8] S. Kuai, A. Meldrum, Rapid color-switching micro-LEDs from silicon MIS diodes, *Phys. E Low-dimens. Syst. Nanostruct.* 41 (2009) 916–919.
- [9] A. Tataroglu, S. Altindal, The analysis of the series resistance and interface states of MIS Schottky diodes at high temperatures using I-V characteristics, *J. Alloys Compd.* 484 (2009) 405–409.
- [10] N.K.R. Nallaba, S. Godavarthi, V.K. Kummara, M.K. Kesarla, D. Saha, H.S. Akkera, G.K. Guntupalli, S. Kumar, S.P. Vattikuti, Structural, optical and photoresponse characteristics of metal-insulator-semiconductor (MIS) type Au/Ni/CeO<sub>2</sub>/GaN Schottky barrier ultraviolet photodetector, *Mater. Sci. Semicond. Process.* 117 (2020) 105190.
- [11] T.K. Le, M. Kang, S.W. Kim, A review on the optical characterization of V<sub>2</sub>O<sub>5</sub> micro-nanostructures, *Ceram. Int.* 45 (2019) 15781–15798.
- [12] M. Uma, M. Siva Pratap Reddy, K. Ravindranatha Reddy, V. Rajagopal Reddy, Electrical and carrier transport properties of Au/Pr<sub>6</sub>O<sub>11</sub>/n-GaN MIS structure with a high-k rare-earth oxide interlayer at high temperature range, *Vacuum* 174 (2020) 109201.
- [13] D.A. Smolyakov, A.S. Tarasov, I.A. Yakovlev, A.N. Masyugin, M.N. Volochaev, I. A. Bondarev, N.N. Kosyrev, N.V. Volkov, Influence of metal magnetic state and metal-insulator-semiconductor structure composition on magnetoimpedance effect caused by interface states, *Thin Solid Films* 671 (2019) 18–21.
- [14] V.R. Reddy, C.J. Choi, Microstructural, chemical and electrical characteristics of Au/magnetite (Fe<sub>3</sub>O<sub>4</sub>)/n-GaN MIS junction with a magnetite interlayer, *Vacuum* 164 (2019) 233–241.
- [15] S.O. Tan, The analysis of the researches on metal-semiconductor structures with and without interfacial layer in Turkey, *Hittite Journal of Science and Engineering* 6 (2019) 51–56.
- [16] S.O. Tan, H. Tecimer, O. Cicek, Comparative investigation on the effects of organic and inorganic interlayers in Au/n-GaAs Schottky diodes, *IEEE Trans. Electron. Dev.* 64 (2017) 984–990.
- [17] B. Ay, O. Sahin, E. Yildiz, One-Pot hydrothermal synthesis of 1D copper (II) coordination polymers involving in-situ decarboxylation, *Solid State Sci.* 96 (2019) 105958.
- [18] A. Baltakesmez, S. Tekmen, B. Guzeldir, Temperature dependent current-and capacitance-voltage characteristics of W/n-Si structures with two-dimensional WS<sub>2</sub> and three-dimensional WO<sub>3</sub> interfaces deposited by RF sputtering technique, *Mater. Sci. Semicond. Process.* 118 (2020) 105204.
- [19] A. Baltakesmez, C. Bilkan, B. Guzeldir, Investigation of electrical and admittance analysis of Au/Thiophene/n-Si structure at room temperature, *Phys. B Condens. Matter* 594 (2020) 412356.
- [20] V. Balasubramani, J. Chandrasekaran, Tien Dai Nguyen, S. Maruthamuthu, R. Marnadu, P. Vivek, S. Sugarthi, Colossal photosensitive boost in Schottky diode behaviour with Ce-V<sub>2</sub>O<sub>5</sub> interfaced layer of MIS structure, *Sensor. Actuator. Phys.* 315 (2020) 112333.
- [21] Y. Tian, Y. Zhou, M. Zhao, Y. Ouyang, X. Tao, Effect of Ce doping on ferroelectric HfO<sub>2</sub> from first-principles: implications for ferroelectric thin films and phase regulation, *J. Solid State Chem.* 328 (2023) 124316.
- [22] M.A. Pinheiro, T.F. Pineiz, E.A. de Morais, L.V. Scalvi, M.J. Saeki, A.A. Cavalheiro, Schottky emission in nanoscopically crystallized Ce-doped SnO<sub>2</sub> thin films deposited by sol-gel-dip-coating, *Thin Solid Films* 517 (2008) 976–981.
- [23] K.H. Prasad, T. Alshahrani, S.J. McCormack, M. Shkir, S. AlFaify, Enhancement in optoelectronic nature of facile spray fabricated Ce co-doped CdO: Zn films for TCO applications, *Optik* 223 (2020) 165408.
- [24] T. Lazar, P. Gowrisankar, E. Selva Esakkil, V. Balaprakash, R. Seeniammal, Fabrication and photosensitivity analysis of MIS Schottky barrier diodes with different molar concentrations of MoO<sub>3</sub> thin films, *Solid State Commun.* 369 (2023) 115194.
- [25] T. Alshahrani, M. Shkir, A. Khan, A.M. El-Toni, A.A. Ansari, M.A. Shar, H. Ghaithan, S. AlFaify, T. Dai Nguyen, V.R.M. Reddy, A remarkable effect of substrate temperature on novel Al/Y<sub>2</sub>O<sub>3</sub>/n-Si heterojunction diodes performance fabricated by facile jet nebulizer spray pyrolysis for optoelectronic applications, *Chin. J. Phys.* 75 (2022) 14–27.
- [26] A. Narmada, P. Kathirvel, Lakshmi Mohan, S. Saravanakumar, R. Marnadu, J. Chandrasekaran, Jet nebuliser spray pyrolysed indium oxide and nickel doped indium oxide thin films for photodiode application, *Optik* 202 (2020) 163701.
- [27] V. Jagadeesan, R. Sakthivel, S. Shanmuga Priya, Improved design and development of an automated jet nebulizer spray pyrolysis system for Ag/Zn:CuO/Si structured diode application, *Mater. Today: Proc.* (2023) <https://doi.org/10.1016/j.matpr.2023.07.329>.
- [28] J. Thangabalu, S. Selvi, J.H. Chang, K. Mohanraj, Impact of substrate temperature on the properties of yttrium oxide thin films prepared by nebulizer spray pyrolysis technique, *Mater. Today: Proc.* 48 (2022) 229–233.
- [29] A. Baltakesmez, Electrical characterization and solar light sensitivity of SnS<sub>2</sub>/n-Si junction, *Journal of the Institute of Science and Technology* 10 (2020) 214–224.
- [30] P. Vivek, J. Chandrasekaran, V. Balasubramani, A. Manimekalai, Insertion of Ga-MoO<sub>3</sub> thin film at Cu/p-Si interface for the fabrication of MIS structure Schottky barrier diodes, *Surface. Interfac.* 37 (2023) 102689.
- [31] M. Hoffmann, U. Schroeder, T. Schenk, T. Shimizu, H. Funakubo, O. Sakata, D. Pohl, et al., Stabilizing the ferroelectric phase in doped hafnium oxide, *J. Appl. Phys.* 118 (2015) 7.
- [32] A. Wei, C. Chen, L. Tang, K. Zhou, D. Zhang, Chemical solution deposition of ferroelectric Sr:HfO<sub>2</sub> film from inorganic salt precursors, *J. Alloys Compd.* 731 (2018) 546–553.
- [33] L. Tang, C. Chen, A. Wei, K. Li, D. Zhang, K. Zhou, Regulating crystal structure and ferroelectricity in Sr doped HfO<sub>2</sub> thin films fabricated by metallo-organic decomposition, *Ceram. Int.* 45 (2019) 3140–3147.
- [34] M. Raj, C. Joseph, M. Subramanian, V. Perumalsamy, V. Elayappan, Superior photo response MIS Schottky barrier diodes with nano porous Sn-WO<sub>3</sub> films for ultraviolet photodetector application, *New J. Chem.* 44 (2020) 7708–7718.
- [35] D. Amram, L. Klinger, N. Gazit, H. Gluska, E. Rabkin, Grain boundary grooving in thin films revisited: the role of interface diffusion, *Acta Mater.* 69 (2014) 386–396.
- [36] R. Siva Prakash, C. Mahendran, J. Chandrasekaran, R. Marnadu, S. Maruthamuthu, I.S. Yahia, M. Shkir, A facile fabrication of Sn-doped CeO<sub>2</sub> nanocrystalline thin films with enhanced photodiode properties for optoelectronic applications, *Appl. Phys. A* 127 (2021) 1–16.
- [37] V. Balasubramani, R. Marnadu, R. Priya, S. Thanikaikaran, A. Sivakumar, M. Shkir, F. Maiz, W.K. Kim, V.R.M. Reddy, Analysis of opto-electrical properties of Cu/Sr-W/n-Si (MIS) Schottky barrier diode for optoelectronic applications, *J. Mater. Sci. Mater. Electron.* 34 (2023) 560.
- [38] H.Y. Shih, M. Shiojiri, C.H. Chen, S.F. Yu, C.T. Ko, J.R. Yang, R.M. Lin, M.J. Chen, Ultralow threading dislocation density in GaN epilayer on near-strain-free GaN compliant buffer layer and its applications in hetero-epitaxial LEDs, *Sci. Rep.* 5 (2015) 13671.
- [39] A.S. Hassanien, A.A. Akl, Crystal imperfections and Mott parameters of sprayed nanostructure IrO<sub>2</sub> thin films, *Phys. B Condens. Matter* 473 (2015) 11–19.
- [40] V. Balasubramani, J. Chandrasekaran, R. Marnadu, P. Vivek, S. Maruthamuthu, S. Rajesh, Impact of annealing temperature on spin coated V<sub>2</sub>O<sub>5</sub> thin films as interfacial layer in Cu/V<sub>2</sub>O<sub>5</sub>/n-Si structured Schottky barrier diodes, *J. Inorg. Organomet. Polym. Mater.* 29 (2019) 1533–1547.
- [41] D. Vasanth Raj, N. Ponpandian, D. Mangalraj, C. Viswanathan, Effect of annealing and electrochemical properties of sol-gel dip coated nanocrystalline V<sub>2</sub>O<sub>5</sub> thin films, *Mater. Sci. Semicond. Process.* 16 (2013) 256–262.
- [42] A. Venkatesan, N.R.K. Chandar, A. Kandasamy, M.K. Chinnu, K.N. Marimuthu, R. Mohan Kumar, R. Jayavel, Luminescence and electrochemical properties of rare earth (Gd, Nd) doped V<sub>2</sub>O<sub>5</sub> nanostructures synthesized by a non-aqueous sol-gel route, *RSC Adv.* 5 (2015) 21778–21785.
- [43] R. Suresh, V. Ponnuswamy, R. Mariappan, N. Senthil Kumar, Influence of substrate temperature on the properties of CeO<sub>2</sub> thin films by simple nebulizer spray pyrolysis technique, *Ceram. Int.* 40 (2014) 437–445.
- [44] Y.T. Park, K.T. Lee, Degradation mechanism of the complementary electrochromic devices with WO<sub>3</sub> and NiO thin films fabricated by RF sputtering deposition, *J. Ceram. Process. Res.* 17 (2016) 1192–1196.
- [45] L.L. Pan, G.Y. Li, J.S. Lian, Structural, optical and electrical properties of cerium and gadolinium doped CdO thin films, *Appl. Surf. Sci.* 274 (2013) 365–370.
- [46] C. Das, J. Begum, S. Choudhury, Effect of thickness on the optical properties of GaAs thin films, *J. Bangladesh Acad. Sci.* 37 (2013) 83–91.
- [47] P. Harishsenthil, J. Chandrasekaran, D. Thangaraju, V. Balasubramani, Fabrication of strontium included hafnium oxide thin film-based Al/Sr: HfO<sub>2</sub>/n-Si MIS-Schottky barrier diodes for tuned electrical behavior, *New J. Chem.* 45 (2021) 19476–19486.
- [48] S. Altindal, A. Barkhordari, S. Ozcelik, G. Pirgholi-Givi, H.R. Mashayekhi, Y. A. Kalandaragh, A comparison of electrical characteristics of Au/n-Si (MS) structures with PVC and (PVC: Sm<sub>2</sub>O<sub>3</sub>) polymer interlayer, *Phys. Scripta* 96 (2021) 125838.
- [49] P. Vidhya, K. Shanmugasundaram, T. Govindaraj, T. Sasikala, V. Balasubramani, N. Senthil Kumar, Fabrication of crack-free PbS thin films by Jet nebulizer spray pyrolysis technique for enhancing optoelectronic applications: an effect of Ce<sup>3+</sup> doping concentrations, *Surface. Interfac.* 42 (2023) 103292.
- [50] P. Velusamy, R.R. Babu, K. Aparna, Effect of Sm doped on the physical properties of ZnO thin films deposited by spray pyrolysis technique, *AIP Conf. Proc.* 1832 (2017) 080085.

- [51] O. Lupon, T. Pauporte, B. Viana, P. Aschehoug, M. Ahmadi, B.R. Cuenya, Y. Rudzevich, Y. Lin, L. Chow, Eu-doped ZnO nanowire arrays grown by electrodeposition, *Appl. Surf. Sci.* 282 (2013) 782–788.
- [52] M. Raja, J. Chandrasekaran, M. Balaji, B. Janarthanan, Impact of annealing treatment on structural and dc electrical properties of spin coated tungsten trioxide thin films for Si/WO<sub>3</sub>/Ag junction diode, *Mater. Sci. Semicond. Process.* 56 (2016) 145–154.
- [53] M.C. Rao, O.M. Hussain, Optical properties of vacuum evaporated WO<sub>3</sub> thin films, *Res. J. Chem. Sci.* 2231 (2011) 606X.
- [54] V. Madhavi, P. Kondaiah, O. M Hussain, S. Uthanna, Structural, optical and electrochromic properties of pure and mo-doped WO<sub>3</sub> films by RF magnetron sputtering, in: Conference Papers in Science, vol. 5, 2013, p. 2013.
- [55] V.D. Mote, J.S. Dargad, B.N. Dole, Effect of Mn doping concentration on structural, morphological and optical studies of ZnO nano-particles, *Nanoscience and Nanoengineering* 1 (2013) 116–122.
- [56] R. Suresh, V. Ponnuswamy, R. Mariappan, Consequence of source material on the surface properties of nebulizer spray coated cerium oxide thin films, *Vacuum* 109 (2014) 94–101.
- [57] Z. Jagoo, Z.A. Lampert, O.D. Jurchescu, L.E. McNeil, Efficiency enhancement of organic thin-film phototransistors due to photoassisted charge injection, *Appl. Phys. Lett.* 7 (2021) 119.
- [58] R. Chauhan, A.K. Srivastava, M. Mishra, K.K. Srivastava, Effect of UV exposure on some optical properties of As-Se based chalcogenide glasses, *Integrated Ferroelectrics Int. J.* 119 (2010) 22–32.
- [59] B. Benhaoua, S. Abbas, A. Rahal, A. Benhaoua, M.S. Aida, Effect of film thickness on the structural, optical and electrical properties of SnO<sub>2</sub>:F thin films prepared by spray ultrasonic for solar cells applications, *Superlattice. Microst.* 83 (2015) 78–88.
- [60] M. Zubair Ansari, N. Khare, Thermally activated band conduction and variable range hopping conduction in Cu<sub>2</sub>ZnSnS<sub>4</sub> thin films, *J. Appl. Phys.* 2 (2015) 117.
- [61] Y. Liu, J. Yu, Wing Man Tang, P.T. Lai, On the voltage dependence of sensitivity for Schottky-type gas sensor, *Appl. Phys. Lett.* 22 (2014) 105.
- [62] R. Marnadu, J. Chandrasekaran, P. Vivek, V. Balasubramani, S. Maruthamuthu, Impact of phase transformation in WO<sub>3</sub> thin films at higher temperature and its compelling interfacial role in Cu/WO<sub>3</sub>/p-Si structured Schottky barrier diodes, *Zeitschrift für Physikalische Chemie* 234 (2020) 355–379.
- [63] J. Mashaiekhy, Z. Shafieizadeh, H. Nahidi, Effect of substrate temperature and film thickness on the characteristics of silver thin films deposited by DC magnetron sputtering, *Eur. Phys. J. Appl. Phys.* 60 (2012) 20301.
- [64] M. Raja, J. Chandrasekaran, M. Balaji, Evaluation of microstructural and electrical properties of WO<sub>3</sub>-x thin films for p-Si/n-WO<sub>3</sub>-x/Ag junction diodes, *Optik* 127 (2016) 11009–11019.
- [65] I. Ahmed, S.-G. Eriksson, E. Ahlberg, Christopher S. Knee, P. Berastegui, L.-G. Johansson, H. Rundlof, et al., Synthesis and structural characterization of perovskite type proton conducting BaZr<sub>1-x</sub>In<sub>x</sub>O<sub>3-δ</sub> (0.0≤x≤0.75), *Solid State Ionics* 177 (2006) 1395–1403.
- [66] C.S. Guclu, E. Erbilen Tanrikulu, A. Dere, S. Altindal, Y.A.S.H.A.R. Azizian-Kalandaragh, A comparison of electrical characteristics of the Au/n-Si Schottky diodes with (ZnCdS: go (1: 1) and (ZnCdS: go (1: 0.5) doped PVP interlayer using current-voltage (I-V) and impedance-voltage (Z-V) measurements, *J. Mater. Sci. Mater. Electron.* 34 (2023) 1909.
- [67] S.O. Tan, H. Uslu Tecimer, O. Cicek, H. Tecimer, I. Orak, S. Altindal, Electrical characterizations of Au/ZnO/n-GaAs Schottky diodes under distinct illumination intensities, *J. Mater. Sci. Mater. Electron.* 27 (2016) 8340–8347.
- [68] N. Kumar, A. Kumari, M. Samarth, R. Kumar, T. Kumar Dey, Analytical studies of metal insulator semiconductor Schottky barrier diodes, *Material Science Research India* 11 (2014) 121–127.
- [69] S. Altindal, H. Kanbur, D.E. Yıldız, M. Parlak, Current conduction mechanism in Al/p-Si Schottky barrier diodes with native insulator layer at low temperatures, *Appl. Surf. Sci.* 253 (2007) 5056–5061.
- [70] S. Karatas, S. Altindal, A. Turut, Muzaffer Çakar, Electrical transport characteristics of Sn/p-Si Schottky contacts revealed from I-V-T and C-V-T measurements, *Phys. B Condens. Matter* 392 (2007) 43–50.
- [71] Z. Tekeli, S. Altindal, M. Cakmak, S. Özçelik, D. Çalışkan, Ekmel Özbay, The behavior of the I-V-T characteristics of inhomogeneous (Ni/Au)-Al<sub>0.3</sub>Ga<sub>0.7</sub>N/AlN/GaN heterostructures at high temperatures, *J. Appl. Phys.* 102 (2007) 5.
- [72] S. Altindal, I. Dökme, M. Mahir Bulbul, N. Yalcin, T. Serin, The role of the interface insulator layer and interface states on the current-transport mechanism of Schottky diodes in wide temperature range, *Microelectron. Eng.* 83 (2006) 499–505.
- [73] I. Dokme, S. Altindal, On the intersecting behaviour of experimental forward bias current-voltage (I-V) characteristics of Al/SiO<sub>2</sub>/p-Si (MIS) Schottky diodes at low temperatures, *Semicond. Sci. Technol.* 21 (2006) 1053.
- [74] S. Zeyrek, S. Altindal, H. Yüzer, M.M. Bulbul, Current transport mechanism in Al/Si<sub>3</sub>N<sub>4</sub>/p-Si (MIS) Schottky barrier diodes at low temperatures, *Appl. Surf. Sci.* 252 (2006) 2999–3010.
- [75] M. Balaji, J. Chandrasekaran, M. Raja, S. Rajesh, Structural, optical and electrical properties of Ru doped MoO<sub>3</sub> thin films and its P-N diode application by JNS pyrolysis technique, *J. Mater. Sci. Mater. Electron.* 27 (2016) 11646–11658.
- [76] E.E. Tanrikulu, Investigation of photon-induced effects on some diode parameters and negative capacitance of the Schottky structure with Zn-doped organic polymer (PVA) interface, *Phys. Scripta* 98 (2022) 015804.
- [77] G. Kalita, M. Kobayashi, M.D. Shaarin, R.D. Mahayavanshi, M. Tanemura, Schottky barrier diode characteristics of graphene-GaN heterojunction with hexagonal boron nitride interfacial layer, *Phys. Status Solidi* 215 (2018) 1800089.
- [78] E.E. Tanrikulu, O. Berkün, M.U.R.A.T. Ulusoy, B. Avar, H. Durmus, S. Altindal, Evaluation of the current transport mechanism depending on the temperature of Schottky structures with Ti: DLC interlayer, *Mater. Today Commun.* 38 (2024) 107992.
- [79] C. Lv, C. Zhu, C. Wang, Dongsheng Li, X. Ma, D. Yang, Defect-related electroluminescence from metal-oxide-semiconductor devices with ZrO<sub>2</sub> films on silicon, *Superlattice. Microst.* 99 (2016) 186–191.
- [80] K. Makoto, T. Oshima, K. Hanada, T. Moribayashi, A. Hashiguchi, T. Oishi, K. Koshi, K. Sasaki, A. Kuramata, O. Ueda, Crystal defects observed by the etch-pit method and their effects on Schottky-barrier-diode characteristics on β-Ga<sub>2</sub>O<sub>3</sub>, *Jpn. J. Appl. Phys.* 56 (2017) 091101.
- [81] P. Harishsenthil, J. Chandrasekaran, R. Marnadu, P. Balraju, C. Mahendran, Influence of high dielectric HfO<sub>2</sub> thin films on the electrical properties of Al/HfO<sub>2</sub>/n-Si (MIS) structured Schottky barrier diodes, *Phys. B Condens. Matter* 594 (2020) 412336.
- [82] H. Elamen, Y. Badali, M. Ulusoy, Y. Azizian Kalandaragh, S. Altindal, M.T. Güneşer, The photo response behaviour of a Schottky structure with a transition metal oxide-doped organic polymer (RuO<sub>2</sub>: PVC) interface, *Polym. Bull.* 81 (2024) 403–422.
- [83] M.A. Salari, M. Saglam, A. Baltakesme, B. Guzeldir, Effect of electron radiation on electrical parameters of Zn/n-Si/Au-Sb and Zn/ZnO/n-Si/Au-Sb diodes, *J. Radioanal. Nucl. Chem.* 319 (2019) 667–678.
- [84] V. Balasubramani, P.V. Pham, A. Ibrahim, J. Hakami, M.Z. Ansari, T.K. Le, Enhanced photosensitive of Schottky diodes using SrO interfaced layer in MIS structure for optoelectronic applications, *Opt. Mater.* 129 (2022) 112449.
- [85] P. Vivek, J. Chandrasekaran, R. Marnadu, S. Maruthamuthu, V. Balasubramani, P. Balraju, Zirconia modified nanostructured MoO<sub>3</sub> thin films deposited by spray pyrolysis technique for Cu/MoO<sub>3</sub>-ZrO<sub>2</sub>/p-Si structured Schottky barrier diode application, *Optik* 199 (2019) 163351.
- [86] R. Marnadu, J. Chandrasekaran, M. Raja, M. Balaji, S. Maruthamuthu, P. Balraju, Influence of metal work function and incorporation of Sr atom on WO<sub>3</sub> thin films for MIS and MIM structured SBDs, *Superlattice. Microst.* 119 (2018) 134–149.
- [87] P. Vidhya, K. Shamugasundaram, P. Thirunavukkarasu, T. Govindaraj, V. Balasubramani, B. Yogeswari, M. Karuppusamy, Enhancement of optoelectronic properties of PbS thin films grown by Jet nebulizer spray pyrolysis technique for photodetector applications: an impact of substrate temperature, *J. Mater. Sci. Mater. Electron.* 34 (2023) 1023.
- [88] K.S. Mohan, R. Marnadu, Yeonju Shin, K.V. Gunavathy, V. Balasubramani, Mohd Ubaidullah, Mohd Shkir, Vasudeva Reddy Minnam Reddy, Kyoung Kim Woo, Substrate heat-assisted spray pyrolysis of crack-free ytterbium sesquioxide-Si heterojunction diodes for photo-sensing applications, *Surface. Interfac.* 39 (2023) 102887.
- [89] P. Paul, Justin, R. Suresh, R. Marnadu, V. Balasubramani, Amelioration of rectification properties of CuO nanostructures using surface modification, *Opt. Mater.* 131 (2022) 112732.
- [90] S. Kalidass, P. Thirunavukkarasu, M. Balaji, J. Chandrasekaran, Investigation on Al doped Zn thin films and its N-Alzno/P-Si junction diodes via dip coating and JNSP techniques, *Orient. J. Chem.* 34 (2018) 2590.
- [91] A. Kaymaz, E.E. Baydilli, H.U. Tecimer, S. Altindal, Y. Azizian-Kalandaragh, Evaluation of gamma-irradiation effects on the electrical properties of Al/(ZnO-PVA)/p-Si type Schottky diodes using current-voltage measurements, *Radiat. Phys. Chem.* 183 (2021) 109430.
- [92] R. Marnadu, J. Chandrasekaran, S. Maruthamuthu, P. Vivek, V. Balasubramani, P. Balraju, Jet nebulizer sprayed WO<sub>3</sub>-Nanoplate arrays for high-photoresponsivity based metal-Insulator-Semiconductor structured Schottky barrier diodes, *J. Inorg. Organomet. Polym. Mater.* 30 (2020) 731–748.
- [93] M. Balaji, J. Chandrasekaran, M. Raja, Role of substrate temperature on MoO<sub>3</sub> thin films by the JNS pyrolysis technique for P-N junction diode application, *Mater. Sci. Semicond. Process.* 43 (2016) 104–113.